CHEMISTRY OF MATERIALS

Article

pubs.acs.org/cm

Understanding and Controlling the Reactivity of the Calcium Silicate phases from First Principles

E. Durgun,*[,†] H. Manzano,[‡,§] R. J. M. Pellenq,[‡] and Jeffrey C. Grossman*[,†]

[†]Department of Materials Science and Engineering and [‡]Department of Civil and Environmental Engineering, Massachusetts Institute of Technology, Cambridge, Massachusetts 02139, United States

Supporting Information

ABSTRACT: First principles calculations are employed to provide a fundamental understanding of the relationship between the reactivity of synthetic calcium silicate phases and their electronic structure. Our aim is to shed light on the wide range of hydration kinetics observed in different phases of calcium silicate. For example, while the dicalcium silicate (Ca_2SiO_4) phase slowly reacts with water, the tricalcium silicate (Ca_3SiO_5) shows much faster hydration kinetics. We show that the high reactivity of Ca_3SiO_5 is mainly related to the reactive sites around its more ionic oxygen atoms. Ca_2SiO_4 does not contain these types of oxygen atoms, although experiments suggest that impurities may play a role in changing the reactivity of these materials. We analyze the electronic structure of a wide range of possible substitutions in both Ca_3SiO_5 and Ca_2SiO_4 and show that while the influence of different types of impurities on structural properties is similar, their effect on reactivity is very different. Our calculations suggest that the variation of electronic structure is mainly related to the formation of new hybridized orbitals and the charge exchange between the impurity atoms and the bulk material. The charge localization upon introducing impurities is quantified to predict candidate substitutions that could increase the reactivity of Ca_2SiO_4, which would broaden the applicability of this lower temperature and thus less costly and energetically less demanding phase.

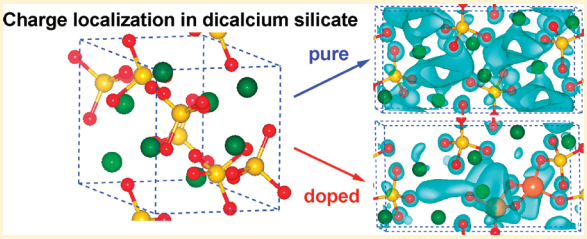

KEYWORDS: *calcium silicate, cement clinker, chemical impurity, reactivity, dissolution*

INTRODUCTION

Calcium silicate is an important component in many minerals and a critical material for wide ranging applications, from building materials such as glass,[1] paint, refractories,[2] and cement,[3,4] to phosphorus materials for light emitting diodes,[5] to pharmaceutical products, cosmetics, and drug delivery[6,7] materials among many others. As a bioactive self-setting material, it is also an appealing candidate for synthetic bone tissue or dental recovery and regeneration.[8−10] Of particular interest is the reaction of calcium silicate-based materials with water, as the hydrated form is heavily used in many of the applications mentioned above. Dicalcium silicate (C_2S), which requires substantially lower manufacturing temperatures, reacts much slower with water than tricalcium silicate (C_3S), rendering it much less useful; yet, to this date we have very little understanding of why certain phases react differently than others, and even less of a clear picture of how to modify or control the hydration. We believe that a more detailed, accurate, and clear understanding is necessary to suggest new paths for controlling the reactivity of these materials.

In this work, we employ first principles techniques to analyze in detail, the structural and electronic properties of two major synthetic calcium silicate components, Ca_2SiO_4 (C_2S) and Ca_3SiO_5 (C_3S), with the particular goal of suggesting methods for increasing reactivity of the lower temperature and thus less costly and more environmentally friendly C_2S. Our calculations help to elucidate the key factors that give rise to the huge difference in reaction rates between these phases. Using this fundamental understanding, we predict the changes in the electronic structure upon introduction of a wide range of foreign impurities, and demonstrate a link between the reactivity profile and the electronic charge density of the considered phases. Our calculations suggest alternative impurities which may be able to control the hydration kinetics of C_2S using simple chemical procedures.

COMPUTATIONAL DETAILS

Our calculations were performed within density functional theory (DFT),[11] using the projector augmented-wave (PAW) method[12] implemented in the VASP package.[13] The exchange-correlation potential was approximated within the generalized gradient approximation (GGA) using the PBE functional.[14] To test the functional dependence of our results, we also carried out calculations using the HSE06 hybrid functional,[15−18] which is constructed by mixing 25% of the Fock exchange with 75% of the PBE exchange and 100% of the PBE correlation energy. The strongly localized 3d-electrons are treated by adding a Hubbard-U term varying from 1 to 3 eV (where U stands for on-site electron−electron repulsion term) into the GGA-PBE functional.[19] The Brillouin zone was sampled with 4 × 4 × 4 k-points in the primitive cell using a plane-wave basis set with a kinetic energy cutoff of 500 eV, which was checked to be sufficient to obtain fully

Received: October 18, 2011
Revised: March 7, 2012
Published: March 29, 2012

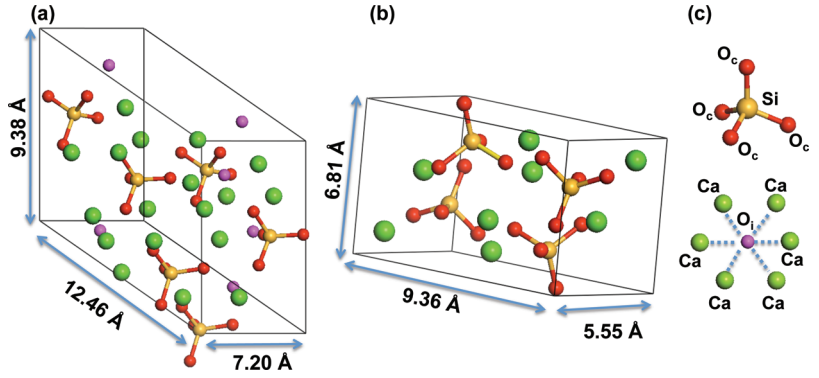

Figure 1. Structure of (a) M3-Ca_3SiO_5 (C_3S) and (b) β-Ca_2SiO_4 (C_2S) and (c) coordination of two types of O atoms. Green, yellow, red, and pink spheres represent Ca, Si, O_i, and O_c atoms, respectively.

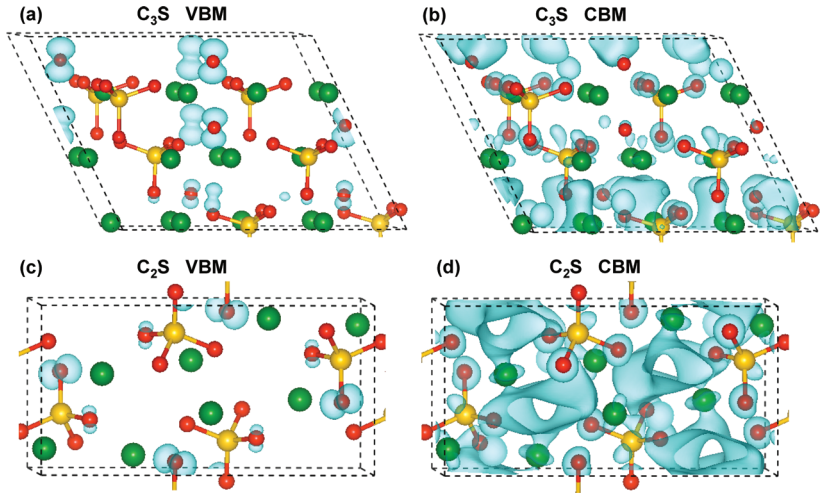

Figure 2. LDOS of the VBM and the CBM for (a), (b) M3-Ca_3SiO_5 (C_3S), and (c), (d) β-Ca_2SiO_4 (C_2S). Green, yellow, and red spheres represent Ca, Si, and O atoms, respectively.

converged results. All structures were relaxed using the conjugate gradient method with simultaneous minimization of the total energy and interatomic forces. The convergence on the total energy was set to 10^{-5} eV, and the maximum residual force allowed on each atom was fixed at 10^{-2} eV/Å.

RESULTS AND DISCUSSION

Among different possible structures for C_3S and C_2S, we mainly focus on the M3-C_3S (CM symmetry group)[20] and β-C_2S (P21/C symmetry group)[21] polymorphs which are the ones most frequently observed in industrial applications. The unit cell and computed lattice parameters of M3-C_3S and β-C_2S consist of 18 Ca, 6 Si, and 30 O (6[Ca_3SiO_5]) and 8 Ca, 4 Si, and 16 O atoms (4[Ca_2SiO_4]), respectively as shown in Figure 1a–b. All of our computed crystal parameters are in good agreement with experimental data.[20−22] Upon comparison, in addition to the well-known Ca to Si ratio (which is 3 for C_3S and 2 for C_2S), another structural difference is evident in the type of oxygen atoms present. The first type (O_c) is covalently bound to silicon atoms forming SiO_4 groups with a bonding distance of 1.61−1.68 Å. The second type (O_i) which only exists in C_3S is interstitial, and ionic in character, surrounded by 5 or 6 Ca atoms, and is loosely bound with a bonding distance of 2.38−2.46 Å as illustrated in Figure 1c. In both cases all Si atoms are part of a silicate group and all Ca atoms are ionic in character.

The concept of local reactivity descriptors, such as the Fukui function,[23−25] is widely used in the context of DFT calculations to investigate the chemical reactivity of a range of systems, ranging from molecules, bulk systems, and surfaces.[26−30] The Fukui function is associated with the differential change in the electron density of a system to an infinitesimal change in the number of electrons under an applied constant external potential $[f(\mathbf{r}) = ((\partial\rho(\mathbf{r}))/(\partial N))_{v(r)}]$. The larger the value of the Fukui function, the greater the reactivity of the corresponding site.[24,25] Three types of Fukui functions can be defined for a system: (1) $f^+(r)$ for nucleophilic attack where the system accepts charge because of an interaction with a nucleophilic reagent. (2) $f^-(r)$ for electrophilic attack where the system donates charge because of interaction with an electrophilic reagent, and (3) $f^0(r)$ for a radical attack approximated as the average of both previous terms. On the basis of frontier orbital theory, considering the highest occupied molecular orbital (HOMO) and lowest unoccupied molecular orbital (LUMO), Fukui functions can be approximately defined as $f^+(r) \sim \rho_{LUMO}(r)$, $f^-(r) \sim \rho_{HOMO}(r)$, and $f^0(r) = 1/2[\rho_{LUMO}(r) + \rho_{HOMO}(r)]$. For bulk systems the HOMO and LUMO are replaced with valence band maximum (VBM) and conduction band minimum (CBM), respectively.[31]

Accordingly we gain insight into the chemical reactivity of C_3S and C_2S (M3-C_3S and β-C_2S have computed energy band gaps of 4.1 and 5.3 eV, respectively) by analyzing the local

dx.doi.org/10.1021/cm203127m | Chem. Mater. 2012, 24, 1262−1267

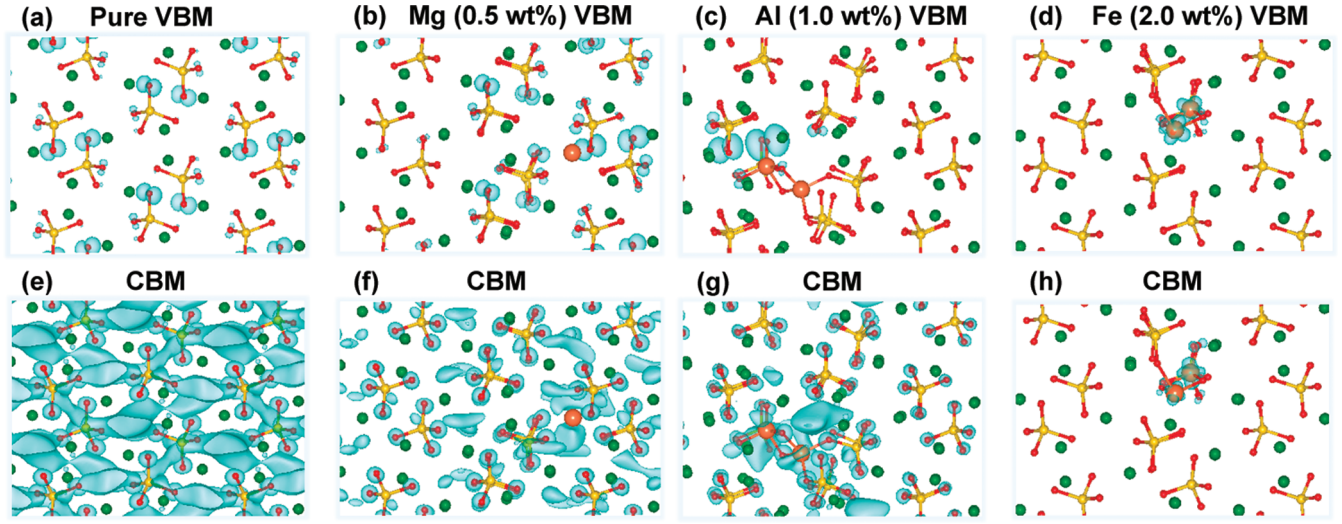

Figure 3. LDOS of the VBM and the CBM for (a), (e) pure, (b), (f) Mg-, (c), (g) Al-, and (d), (h) Fe-doped β-Ca_2SiO_4 (C_2S). Green, yellow, red, and orange spheres represent Ca, Si, O, and impurity atoms, respectively. The impurity concentrations are given in parentheses.

density of states (LDOS) of the VBM and the CBM as they can provide a reactivity profile of the system and site selectivity of a reaction. The LDOS of the VBM is accumulated around O_i for C_3S whereas it is around O_c (on the silicate group) for C_2S as shown in Figure 2. Consequently, the regions of both types of oxygen atoms exhibit a trend to lose electrons, which makes them susceptible to undergo electrophilic attack. Since O_i atoms are loosely bound to the system compared to O_c atoms, our calculations suggest that they will form oxides more easily with electrophile cations such as, H^+, Na^+, Mg^{2+}, and Ca^{2+}. On the other hand, the LDOS for the CBM is delocalized especially for C_2S, dispersed to the regions between the Ca and SiO_4 groups and slightly accumulated on O atoms for *both* phases as shown in Figure 2. Thus, there are no significant regions that are more reactive to nucleophilic attack (e.g., SO_4^{-2}, OH^-) which can influence the reactivity rates. These results therefore suggest that the more ionic character, active O_i atoms and higher Ca/Si ratio, of C_3S plays the key role in its fast reactivity with water when compared to C_2S.

With this understanding of the pure phases, we now turn our attention to possible ways to increase the ionic character of C_2S to increase its reactivity with water. As C_2S does not contain any of the O_i type atoms, one alternative method would be to modify the delocalized nature of the CBM by introducing impurities that cause the material to accumulate more charge in specific regions, especially around ionic Ca atoms. An ideal impurity for increasing reactivity should partially localize the LDOS of the CBM allowing more charge accumulation around some of the Ca atoms without completely localizing all the charge on the impurity, as this will dramatically reduce the already existing reactive sites. We begin with Mg, Al, and Fe as the foreign oxides MgO, Al_2O_3, and Fe_2O_3 are commonly found in calcium silicate phases, and considered the substitutions Ca by Mg and Ca+Si by 2 Al or 2 Fe atoms, taking into account charge balance. The typical and maximum amount of such impurities vary with the type of atom and calcium silicate phase.[32] Thus, we employ classical force field calculations[33] to explore a wide range of substitution levels, from 0.2 to 8 wt %, to identify favorable substitutions sites. An analysis of these results, considering all possible sites, revealed that the total energy varies with substitution site but does not follow a clear trend.[34]

Our calculations show that structural and mechanical properties of C_2S and C_3S are only slightly affected and moreover in the same manner upon introduction of impurities at different doping levels.[34] This reinforces our earlier postulate that the dramatic difference in the reactivity of C_2S and C_3S is mainly related to their electronic structure and does not follow the same trend as the mechanical properties. The change in the LDOS of both the CBM and VBM is shown in Figure 3 for the introduction of Mg, Al, and Fe impurities at ~0.5, 1, and 2% doping concentrations. Compared to pure C_2S, the delocalized LDOS of the CBM is altered upon Mg and Al substitution and accumulated on O_c atoms and around the impurities. The localization effect is stronger for the case of Al, forming a region where most of the charge is accumulated around the Al atom that substitutes Ca, resulting in a more reactive region for nucleophilic attack. The LDOS of the VBM is still accumulated on O_c atoms upon Mg and Al substitution although more localized on the ones near the impurities. This change may increase the reactivity of silicate groups near the impurity at the cost of decreasing the number of sites that can interact with electrophile cations. The picture is more dramatic for Fe, where all of the LDOS of the CBM and VBM is concentrated on the Fe atoms, essentially eliminating all the reactive regions. The effect of impurities on the electronic structure is enhanced with increasing doping level for all three impurities. Note that although Figure 3 shows results for substitutions in C_2S, our calculations indicate similar trends for the same impurities substituted in C_3S (see Supporting Information).

The diverse variation in electronic structure upon introduction of different types of dopants can be explained by analyzing the charge transfer and bonding character of the impurities with surrounding atoms. A Bader analysis[35−37] indicates that the net charge on Mg atoms is +1.72e where it is on average +1.55e on Ca atoms. Thus even though Mg and Ca have the same valence electronic configuration, each Mg atom gives approximately +0.17e more charge to the system. A partial density of states (PDOS) analysis (see Supporting Information) shows that while the LDOS of the VBM is mainly dominated by O-p orbitals, a strong hybridization between the Mg-s and O-sp

dx.doi.org/10.1021/cm203127m | *Chem. Mater.* 2012, 24, 1262−1267

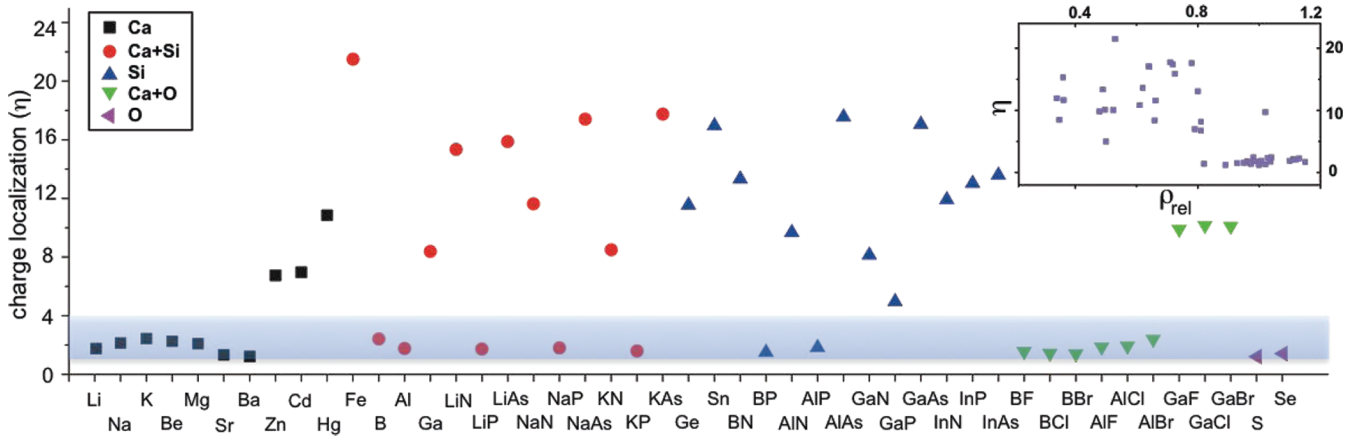

Figure 4. Variation of charge localization (η) with type of impurity atoms or pairs. The highlighted region corresponds to the interval ($1 < \eta < 4$) where partial localization occurs that could lead to enhanced reactivity. The inset shows the variation of η with relative Bader charge (ρ_{rel}) which is equal to $\Delta\rho_{impurity}/\Delta\rho_{reference}$ where $\Delta\rho_{impurity}$ and $\Delta\rho_{reference}$ are the average Bader charge of impurity atom or pair and the substituted reference atom (Ca, Si, O) or pair (Ca+Si, Ca+O, Si+O), respectively.

changes the nature of the CBM state, which together with the extra charge transfer explains the partial localization of the LDOS around Mg. In the case of Al substitution, two Al atoms transfer 4.84e to the system while each Ca (1.53e) and Si (3.08e) together transfer 4.61e to the system in the pure phase. Thus, similar to the Mg case, each Al atom donates more charge (on average 0.12e) but in this case as the Al pair substitutes both Ca and Si, the asymmetry induces a stronger partial localization. The Al-s, O-sp, and Ca-s orbitals contribute to the LDOS of the CBM. For the case of Fe, two Fe atoms donate 2.42e instead of 4.61e (Ca+Si) and thus reduce the charge transferred to the system per impurity atom by 1.10e. The PDOS analysis indicates that while the electrons from Fe-s orbitals are distributed among the whole unit cell, Fe-d orbitals strongly hybridize with O-p orbitals and charge is completely localized around the Fe atoms.

Thus far, our results are encouraging regarding the original motivation of increasing the reactivity of C_2S, since the electronic structure clearly shows a strong dependence on introduction of impurities. Experimentally, a recent study[38] reports increased hydration kinetics for Al doped C_2S and slow reactivity upon substitution of Fe, which supports our predictions of reactivity based on the changes in electronic structure. In the case of C_3S, there are contradictory experimental studies suggesting both an acceleration[39] and slowing down[40] with Al substitution. Similarly, a slight increase,[39] decrease[41] or no change[42] in reactivity is reported upon MgO incorporation into C_3S. These discrepancies could be due to differences in the measurement techniques or experimental conditions, such as the cooling rate, particle size, and molar ratios. According to our predictions, the reactivity of C_3S should not vary much with Mg incorporation, as it does not alter the electronic structure with respect to the pure phase. Fe substitutions significantly reduce the reactive sites via complete localization of both the VBM and CBM, in good agreement with all experimental findings.[38,39,42]

Using the understanding gained in the above analysis of Mg, Al, and Fe doped C_2S and C_3S, we next turn to the prediction of alternative impurities that could modify the electronic structure, and try to quantify the obtained results toward our original goal of increasing the reactivity of C_2S. We explored a vast range of impurities by substituting (i) Ca by alkali and earth alkali atoms, (ii) Si by group IV and III−V atoms, (iii) Ca+Si by group III and I−V atoms, (iv) Si+O by group III−VII atoms, (v) Ca+O by group I−VII atoms, and (vi) O by group VI atoms. A complete list of substitutions is shown in Figure 4.

As the partial charge localization of the VBM and CBM play a key role in predicting the influence of a given impurity on reactivity, we attempt here to quantify the localization. In our calculations, the VBM and CBM correspond to separate bands each of which holds 2e spread over the cell volume. The LDOS plots in Figure 3 correspond to the charge normalized over the volume. Accordingly, since both the charge and volume are fixed, the maximum isosurface value (MIV) (in units of e/Å^3) increases with localization, and a comparison of MIV-pure and MIV-doped phases should represent the trend of how the spread of charge changes with respect to the pure phase. We define the localization (η) as the ratio MIV-doped/MIV-pure and consider $\eta = 1$ for the pure case. The computed values of η for all the substitutions considered are shown in Figure 4. According to our definition $\eta = 1$ corresponds to no localization, and an LDOS analysis of the CBM points out that $\eta > 4$ corresponds to complete localization on the impurity atom(s). Thus, we can postulate that a region of η that could lead to enhanced reactivity would be $1 < \eta < 4$ which is therefore highlighted in Figure 4. By this analysis we are able to eliminate the substitutions which would clearly decrease reactivity because of strong localization, and also identify possible candidates which may increase reactivity. As can be seen in Figure 4, some candidate substitutions for enhancing reactivity based on our calculations would be Li, K (alkali), Be, Sr (earth alkali), B, Al (group III) and BP, AlP (group III−V), and LiP (group I−VII).

As already discussed, this localization trend of the CBM is mainly related to the electron exchange between the impurity atom and the rest of the system. To quantify the charge localization with respect to charge donation/gain ($\Delta\rho$), we defined a relative Bader charge (ρ_{rel}) which is equal to $\Delta\rho_{impurity}/\Delta\rho_{reference}$ where $\Delta\rho_{impurity}$ and $\Delta\rho_{reference}$ are the average Bader charge of the impurity atom or pair and the substituted reference atom (Ca, Si, O) or pair (Ca+Si, Ca+O, Si+O), respectively. The inset in Figure 4 clearly indicates that the candidate impurities (for which partial localization is observed) lie in the region $\sim \pm 20\%$ of $\rho_{rel} = 1$. In a similar manner if the impurity atom holds its charge (except group VI and VII elements) and consequently donates significantly less

dx.doi.org/10.1021/cm203127m | Chem. Mater. 2012, 24, 1262−1267

charge than the substituted atom, then the density is mainly accumulated on the impurity atom and complete localization occurs.

The PDOS analysis indicates that, except for Fe, while the valence states close to the Fermi level are only slightly affected by impurity doping, the conduction states are significantly modified. For the cases where strong charge localization (or high η values) occurs, the common feature is the formation of new conduction states upon hybridization of impurity-s, calcium-s, and oxygen-p orbitals. Partial charge localization occurs when the Ca and impurity contributions are balanced, and complete localization occurs when the impurity contribution starts to dominate. Fe is exceptional, as it also contains valence d-electrons that strongly hybridize and thus strongly alter both the valence and the conduction states. Another interesting feature is the variation of the electronic band gap which is inversely proportional to η. Upon formation of new valence states, the electronic band gap closes when compared to pure C_2S, and charge localization increases. The system becomes almost metallic for the Fe case where the strongest localization is observed (see Supporting Information).

It is important to note that although our detailed electronic structure analysis of various impurity combinations sheds light on important fundamental aspects of the reactivity profile of calcium silicate phases, additional effects could also play an important role. For example, defects in addition to impurity substitutions, surface reconstruction in addition to bulk surfaces, and solvent effects (such as water) in addition to a vacuum environment should also be considered.

CONCLUSION

In conclusion, we used density functional theory calculations to provide a fundamental link between the reactivity of the calcium silicate phases and their electronic structure. We showed that the high reactivity of C_3S is mainly related to the reactive sites around the more ionic oxygen atoms which are loosely bound to the system. Our calculations show that while the influence of different types of impurities on structural properties is similar for C_2S and C_3S, their effect on the electronic structure is very different. These differences are shown to influence the reactivity in these materials, and good agreement with available experimental data is demonstrated. By quantifying the charge density localization of the VBM and CBM for a large set of potential substitutions, we predict several candidates that could influence the reactivity of C_2S. It is our belief that the kind of fundamental understanding gained here, which relates the reactivity of the building blocks of many minerals to chemical substitutions can help to accelerate and guide future theoretical, experimental, and industrial research toward high performance materials with desired properties.

ASSOCIATED CONTENT

Supporting Information

Figures of LDOS of the VBM and the CBM for pure and doped Ca_3SiO_5 (C_3S), functional dependence of the charge localization parameter (η) and Bader charges for selected impurities, the variation of electronic band gap by type of impurity atoms or pairs, and the total density of states of pure and doped Ca_2SiO_4 (C_2S) are shown. This material is available free of charge via the Internet at http://pubs.acs.org.

AUTHOR INFORMATION

Corresponding Author

*E-mail: edurgun@mit.edu (E.D.), jcg@mit.edu (J.C.G.).

Present Address

[§]Laboratory for Molecular Spectroscopy, UPV/EHU.

Notes

The authors declare no competing financial interest.

ACKNOWLEDGMENTS

This work has been supported by the Concrete Sustainability Hub at MIT, with sponsorship provided by the Portland Cement Association (PCA) and the RMC Research and Education Foundation. H.M. acknowledges the postdoctoral grant received by the Department of Education, Science and Universities of the Basque Country Government. This research used Teragrid resources, which are supported by the National Science Foundation under Grants TG-DMR090027 and TG-DMR110027.

REFERENCES

(1) Eckersley, M. C.; Gaskell, P. H.; Barnes, A. C.; Chieux, P. *Nature* **1988**, *335*, 525−527.

(2) Rodriguez, J.; Rodriguez, M.; Aza, S. D.; Pena, P. *J. Eur. Ceram. Soc.* **2001**, *21*, 343−354.

(3) Allen, A. J.; Thomas, J. J.; Jennings, H. M. *Nat. Mater.* **2007**, *6*, 311−316.

(4) Pellenq, R. J.-M.; Kushima, A.; Shahsavari, R.; Van Vliet, K. J.; Buehler, M. J.; Yip, S.; Ulm, F.-J. *Proc. Natl. Acad. Sci. U.S.A.* **2009**, *106*, 16102−16107.

(5) Kim, J. S.; Park, Y. H.; Kim, S. M.; Choi, J. C.; Park, H. L. *Solid State Commun.* **2005**, *133*, 445−448.

(6) Cai, Y.; Pan, H.; Xu, X.; Hu, Q.; Li, L.; Tang, R. *Chem. Mater.* **2007**, *19*, 3081−3083.

(7) Xu, Q.; Tanaka, Y.; Czernuszka, J. T. *Biomaterials* **2007**, *28*, 2687−2694.

(8) Constantz, B.; Ison, I.; Fulmer, M.; Poser, R.; Smith, S.; VanWagoner, M.; Ross, J.; Goldstein, S.; Jupiter, J.; Rosenthal, D. *Science* **1995**, *267*, 1796−1799.

(9) Ding, S.-J.; Shie, M.-Y.; Wang, C.-Y. *J. Mater. Chem.* **2009**, *19*, 1183−1190.

(10) Aza, P. D.; Fernandez-Pradas, J.; Serra, P. *Biomaterials* **2004**, *25*, 1983−1990.

(11) (a) Kohn, W.; Sham, L. J. *Phys. Rev.* **1965**, *140*, A1133−A1138. (b) Hohenberg, P.; Kohn, W. *Phys. Rev.* **1964**, *136*, B864−B871.

(12) Blöchl, P. E. *Phys. Rev. B* **1994**, *50*, 17953−17979.

(13) (a) Kresse, G.; Hafner, J. *Phys. Rev. B* **1993**, *47*, 558−561. (b) Kresse, G.; Furthmuller, J. *Phys. Rev. B* **1996**, *54*, 11169−11186.

(14) Perdew, J. P.; Burke, K.; Ernzerhof, M. *Phys. Rev. Lett.* **1996**, *77*, 3865−3868.

(15) Becke, A. D. *J. Chem. Phys.* **1996**, *104*, 1040−1046.

(16) Paier, J.; Hirschl, R.; Marsman, M.; Kresse, G. *J. Chem. Phys.* **2005**, *122*, 234102.

(17) Paier, J.; Marsman, M.; Hummer, K.; Kresse, G.; Gerber, I. C.; Ángyán, J. G. *J. Chem. Phys.* **2006**, *124*, 154709.

(18) Heyd, J.; Scuseria, G. E.; Ernzerhof, M. *J. Chem. Phys.* **2006**, *124*, 219906.

(19) Dudarev, S. L.; Botton, G. A.; Savrasov, S. Y.; Humphreys, C. J.; Sutton, A. P. *Phys. Rev. B* **1998**, *57*, 1505−1509.

(20) de Noirfontaine, M.-N.; Dunstetter, F.; Courtial, M.; Gasecki, G.; Signes-Frehel, M. *Cem. Concr. Res.* **2006**, *36*, 54−64.

(21) Fukuda, K.; Ito, S. *J. Am. Ceram. Soc.* **1999**, *82*, 2177−2180.

(22) The experimental lattice parameters are a = 5.51 Å, b = 6.75 Å, c = 9.30 Å, β = 94.59° for C_2S[21] and a = 9.30 Å, b = 7.08 Å, c = 12.22 Å, β = 116.08° for C_3S.[20]

(23) Holton, J.; Lappert, M. F.; Pearce, R.; Yarrow, P. I. W. *Chem. Rev.* **1983**, *83*, 135−201.

(24) Parr, R. G.; Yang, W. *J. Am. Chem. Soc.* **1984**, *106*, 4049−4050.
(25) Chattaraj, P. K. *Chemical Reactivity Theory: a Density Functional View*; Taylor & Francis/CRC Press: Boca Raton, FL, 2009.
(26) Parr, R. G.; Yang, W. *Density-Functional Theory of Atoms and Molecules*; Oxford University Press: New York, 1989.
(27) Cárdenas, C.; Proft, F. D.; Chamorro, E.; Fuentealba, P.; Geerlings, P. *J. Chem. Phys.* **2008**, *128*, 034708.
(28) Geerlings, P.; De Proft, F.; Langenaeker, W. *Chem. Rev.* **2003**, *103*, 1793−1874.
(29) Santos, J. C.; Chamorro, E.; Contreras, R.; Fuentealba, P. *Chem. Phys. Lett.* **2004**, *383*, 612−616.
(30) Manzano, H.; Dolado, J. S.; Ayuela, A. *J. Am. Ceram. Soc.* **2009**, *92*, 897−902.
(31) The main advantage of the method is that it is based on the true many-body electron density including electron correlation effects, but the localization and delocalization errors of DFT functionals which generally tend to overstabilize subsystems with fractional numbers of electrons, and thus favor delocalizing the Fukui function over the entire system, should be taken into account.
(32) Taylor, H. F. W. *Cement Chemistry*, 2 ed.; Thomas Telford: London, U.K.; 1997.
(33) (a) Gale, J. D. *J. Chem. Soc., Faraday Trans.* **1997**, *93*, 629−637. (b) Gale, J. D.; Rohl, A. L. *Mol. Simul.* **2003**, *29*, 291−341.
(34) Manzano, H.; Durgun, E.; Abdolhosseine Qomi, M. J.; Ulm, F.-J.; Pellenq, R. J. M.; Grossman, J. C. *Cryst. Growth. Des.* **2011**, *11*, 2964−2972.
(35) Bader analysis is a method to divide molecules into atoms using a partitioning of the electron charge density. A zero flux surface where the charge density reaches its minimum is considered as a region to separate atoms. Bader analysis is useful to calculate various physical and chemical properties of a system including partial charges of atoms. The partial charge concept is not uniquely defined and depends on the method. In that sense Bader charge analysis is a good approximation method to calculate electronic charge of an atom in a system within a volume called Bader volume.
(36) Bader, R. F. W. *Chem. Rev.* **1991**, *91*, 893−928.
(37) Tang, W.; Sanville, E.; Henkelman, G. *J. Phys.: Condens. Matter* **2009**, *21*, 084204.
(38) Kim, Y.-M.; Hong, S.-H. *J. Am. Ceram. Soc.* **2004**, *87*, 900−905.
(39) Stephan, D.; Wistuba, S. *J. Eur. Ceram. Soc.* **2006**, *26*, 141−148.
(40) Odler, I.; Schuppstuhl, J. *Cem. Concr. Res.* **1981**, *11*, 765−774.
(41) Thompson, R. A.; Killoh, D. C.; Forrester, J. A. *J. Am. Ceram. Soc.* **1975**, *58*, 54−57.
(42) Abdul-Maula, S.; Odler, I. *Proc. Br. Ceramic Soc.* **1984**, *35*, 83.